Synthesis and Characterization of Ultrahigh Crystalline TiO_2 Nanotubes

M. Alam Khan,[†] Hee-Tae Jung,[‡] and O-Bong Yang*[,†]

School of Environmental and Chemical Engineering, Center for Advanced Radiation Technology, Chonbuk National University, Jeon-Ju 561-756, Korea, and Department of Bioengineering and Chemical Engineering, Korea Advanced Institute of Science and Technology (KAIST), Dae-Jeon, Korea

Received: December 7, 2005; In Final Form: February 3, 2006

Ultrahigh crystalline TiO_2 nanotubes were synthesized by hydrogen peroxide treatment of very low crystalline titania nanotubes (TiNT-as prepared), which were prepared with synthesized TiO_2 nanoparticles by hydrothermal methods in an aqueous NaOH solution. Thus, prepared ultrahigh crystalline TiO_2 nanotubes (TiNT-H_2O_2) showed comparable crystallinity with high crystalline TiO_2 nanoparticles. The details of nanotubular structures were elucidated by high resolution-transmission electron microscopy (HR-TEM), field emission-scanning electron microscopy (FE-SEM), energy-dispersive X-ray analysis in transmission electron microscopy (TEM-EDX), X-ray diffraction (XRD), photoluminescence (PL), and BET surface area. TiNT-H_2O_2 was found to be a multiwalled anatase phase only with an average outer diameter of ∼8 nm and an inner diameter of ∼5 nm and grown along the [001] direction to 500−700 nm long with an interlayer fringe distance of ca. 0.78 nm. The photocatalytic activity of TiNT-H_2O_2 was about 2-fold higher than those of TiNT-as prepared, synthesized TiO_2 nanoparticles, and TiO_2−P25 (Degussa) in the photocatalytic oxidation of trimethylamine gas under UV irradiation.

Introduction

Since the pioneering work on the applications of titanium dioxide (TiO_2) as photocatalytic[1] and photovoltaic[2] materials, TiO_2 has been studied extensively for various purposes. Fine TiO_2 semiconductor materials are ideal due to their chemical stability, nontoxicity, and high photocatalytic reactivity and are widely used in the elimination of pollutants,[3] gas sensing,[4,5] and fabrication of solar cells.[6] The physicochemical properties of nanomaterials are dependent on their structural properties such as size, shape, and crystallinity. For example, fine TiO_2 semiconductor nanoparticles less than 10 nm show significant enhancement in photocatalytic activity by quantum size effects.[7]

Recently, there have been extensive studies on nanostructured tubular materials because of their exceptional physical properties[8,9] and potential applications in nanoelectronics.[10] Relatively, the titania nanotubes have not been intensively studied, and works on its modification are not explored well, despite the potential advantage to providing direct conduction paths for the photoexcited electrons through the tube channel. Titania nanotubes were synthesized by Hoyer[11] with anodic porous alumina, which possessed a diameter of 70−100 nm, low surface area, and polycrystallinity. Also, Kasuga et al.[12] reported on the synthesis of high surface area titanium dioxide nanotubes with very low crystallinity by aqueous NaOH treatment of titania nanoparticles. Du et al.[13] reported on the titanate ($H_2Ti_3O_7$) nanotube neither anatase nor rutile phase with very low crystallinity. Despite the previous studies in favor of the synthesis of titania nanotubes for its excellent morphology, these low crystalline TiO_2 nanotubes have significant limitations as advanced materials in photoinduced reactions, due to their low activity.[14,15] It has been known that defects in low crystalline TiO_2 may act as recombination sites of generated electrons and holes.[16] On the contrary, unique optical and electrical properties of high crystalline metal oxide nanotubules have been well-documented.[17] Thus, the titania nanotubes with a high crystallinity and high surface area are expected to be promising materials with noble photocatalytical, electrical, and optical properties. However, far less effort has been focused on the development of such high crystalline titania nanotubes, despite their technological importance. In this work, we first demonstrate the simple chemical synthesis of ultrahigh crystalline TiO_2 nanotubes as high as crystalline TiO_2 nanoparticles. Detailed structural and photocatalytical properties of the titania nanotubes were elucidated. To our best knowledge, the preparation of ultrahigh crystalline TiO_2 nanotubes by controlled chemical treatment has not yet been documented.

Experimental Procedures

Titania Nanotube Synthesis. For the synthesis of titania nanotubes, TiO_2 nanoparticles were prepared as follows: the first mixture of a TiO_2/SiO_2 mole ratio of 90:10 obtained by mixing 52 mL of titanium isopropoxide (TTIP, Ti [OCH$(CH_3)_2]_4$, > 99%, Junsei Chemical Co.) and 5.2 mL of tetraethyl orthosilicate (TEOS, Si$(OC_2H_5)_4$, > 99%, Acros Organics), was dissolved in 52 mL of ethanol (99.5%). After refluxing the first mixture solution at room temperature for 1 h, the second mixture of 52 mL of ethanol and 40.6 g of 4 M aqueous HCl (36%, Showa Chemical Co.) was added slowly to the first mixture solution and further stirred at room temperature for 1 h. To form the precipitation of xerogel, the prepared sol was placed into the incubator at 80 °C for 48 h. Then, xerogel was dried and calcined in air at 600 °C for 3 h, which became the high crystalline TiO_2 nanoparticles (denoted as the synthesized TiO_2 nanoparticles in this text) with an anatase phase and ca. 20 nm size. To synthesize titania nanotubes (TiNTs) by hydrothermal methods, the prepared and pulverized TiO_2 nanoparticle powders

* Corresponding author. E-mail: obyang@chonbuk.ac.kr. Phone: + 82-63-270-2313. Fax: + 82-63-270-2306.
[†] Chonbuk National University.
[‡] Korea Advanced Institute of Science and Technology.

10.1021/jp057119k CCC: $33.50
Published on Web 03/16/2006

(<38 μm) were treated by an 8 M NaOH aqueous solution in an autoclave with a Teflon lined high-pressure stainless steel vessel at 130 °C and ambient pressure for 20 h. After cooling to room temperature, the precipitated powders were filtrated and washed with 0.1 N aqueous HCl solutions and distilled water, until the filtrate reached pH < 7. The filtrated and washed powders were dispersed through sonication for 10 min and dried at ambient temperature. This resulting sample was a titania nanotube and denoted as TiNT-as prepared. For the synthesis of ultrahigh crystalline TiO_2 nanotubes, the TiNT-as prepared powders were treated by the 2 wt % hydrogen peroxide (Aldrich, 99.9%) aqueous solutions under refluxing conditions at 40 °C for 4 h. The powders were filtrated and washed with distilled water and dried in an oven at 80 °C for 6 h. This resulting sample was ultrahigh crystalline titania nanotubes and represented as TiNT-H_2O_2. For characterization and catalysis, all of the TiNTs were used after calcining in air at 350 °C for 2 h.

Characterization. The details of the structure and morphology of titania nanotubes were examined by field emission scanning electron microscopy (FE-SEM, Hitachi 4700), high-resolution transmission electron microscopy (HR-TEM, Philips Technai 160 kV, three focused step, bright field), X-ray diffraction (XRD, Rigaku, with Cu Kα radiation), energy-dispersive X-ray analysis in TEM (TEM-EDX, JEOL JEM-2010, high voltage range of 80−200 kV), X-ray photoelectron spectroscopy (XPS, Perkin-Elmer, PHI 5400, Al Kα radiation), photoluminescence (PL, Flourospectroscopy 15S), and BET surface area (Micromeritics ASAP 2100).

Photocatalytic Activity Test. The oxidation of trimethylamine ($N(CH_3)_3$, TMA) gas was conducted for the comparison of photocatalytic activities of TiNTs under UV (254 nm) irradiation in a quartz tube reactor (240 mm height × 28 mm i.d.). TiNTs powders were immobilized on a glass plate as follows: the slurry of TiNTs was prepared by mixing 2 g of TiNTs with 5 mL of distilled water and coated through the doctor blade method on both sides of the slide glass plate (236 mm length × 26 mm width). The amount of coated TiNTs was controlled and kept ca. 1 g. After the plate dried at room temperature, the plate was installed horizontally in a center of the quartz tubular reactor. Two UV lamps (254 nm, 15 W) were placed parallel to the coated face of the plate. The reactor was flushed by flowing He for 30 min, and the reactant mixture (200 ppm TMA, 20% O_2 and 80% N_2) was introduced into the reactor (100 mL/min). After the gas−solid adsorption equilibrium was achieved by flowing through the reactant mixture for 10 min, the UV lamps were switched on to start the reaction. The reactant and products were analyzed by the on-line quadruple mass spectrometer (Balzers QMS200).

Results and Discussion

Figure 1 shows the TEM and FE-SEM (inset) images of TiO_2 nanotubes before (TiNT-as prepared) and after (TiNT-H_2O_2) treatment of hydrogen peroxide. There are no clear differences in the physical appearance of the nanotubues between TiNT-as prepared and TiNT-H_2O_2, which grew extensively with a length of 500−700 nm with quite clean tubular surfaces and no breakages except a yellow plate color in TiNT-H_2O_2 due to the presence of a peroxo group. This yellow color vanished after heat treatment at 250 °C. In the HR-TEM images (Figure 1), TiNTs were both hollow nanotubes with an ∼8 nm o.d. and ∼5 nm i.d. before (Figure 1a) and after (Figure 1b) treatment of hydrogen peroxide. However, the morphology of TiNT-H_2O_2 grew more uniform and linear than that of TiNT-as prepared. On viewing down the direction perpendicular to the channel axis in TiNT-H_2O_2, the walls were thick and contained many layers, as one side was slightly thicker than the other. The electron micrograph projected along the channel axis presented a scroll structure, which suggests that the titania nanotubes were formed by the rolling of a single sheet of titanium oxide. Figure 2 represents the high magnification HR-TEM images of single TiNT-H_2O_2. Two types of lattice fringes are observed as shown in Figure 2b,c. The fringes parallel to the longitudinal direction of the tube axis with an ca. 0.78 nm interplannar distance correspond to the structural features of cis-skewed chains, which are characteristics of the anatase phase in the (001) direction.[18] Another set of fringes toward tube periphery with ca. 0.38 nm spacing is assigned to the (101) plane of the anantase crystal structure. The formation of TiO_2 nanotubes with NaOH solution may be explained by the following mechanisms. Few of Ti−O−Ti building units in TiO_2 particles are broken and formed Ti−O−Na and Ti−OH. To form the Ti−O−Ti dimmer by sharing edges, sodium ions and hydroxyl groups in the Ti−O−Na and Ti−OH bonds are removed by the reaction of acids and water.[19] These dimmers are condensed to form skewed chains as a result of an oblation process[20] due to partial charge.[21] The anatase surface energy can be quenched easily in the hydrothermal treatment process due to less surface energy, which causes preferable growth for the anatase phase ($a = b \approx 3.78$ Å, $c \approx 9.25$ Å with a longer c axis) rather than rutile phase in titania nanotubes.[22]

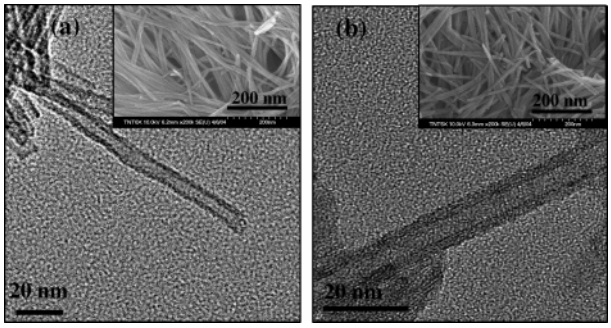

Figure 1. FE-SEM (inset) and TEM images of (a) TiNT-as prepared and (b) TiNT-H_2O_2.

On the selected area electron diffraction (SAED) patterns in Figure 3, TiNT-as prepared and TiNT-H_2O_2 are composed of anatase structural building units with the phases of (101), (004), and (200) from the core of the nanotube. It is obvious that primary and secondary spots of TiNT-H_2O_2 are more prominent than those of TiNT-as prepared where the spots are not distinct. Other phases in TiNT-H_2O_2 are not clearly observed in TiNT-as prepared. This SAED result suggests that the structure of TiNT-H_2O_2 is more uniform and crystalline as compared to TiNT-as preapred.

XRD patterns of TiNTs (Figure 4) exhibit the typical characteristics of TiO_2 with only the anatase phase. It is notable that the crystallinity of TiNTs was drastically increased by the chemical treatment of TiNT-as prepared with 2 wt % aqueous hydrogen peroxide without affecting the physical morphology of the nanotubes. In comparison to the main XRD peak of (101), the relative intensities of TiO_2 nanoparticle/TiNT-H_2O_2/TiNT-as prepared are 6.6:6.0:1.0. TiO_2 nanoparticles herein were prepared by the sol−gel method and calcined at 600 °C for the synthesis of TiNT-as prepared. To our knowledge, the synthesis of such ultrahigh crystalline titania nanotubes as comparable to the high crystalline anatase titania particles by simple chemical treatment has not been reported.[10,11] There is only the anatase phase without any rutile phase, which contrasts with Du et al.,[11] where they observed both anatase and rutile phases.

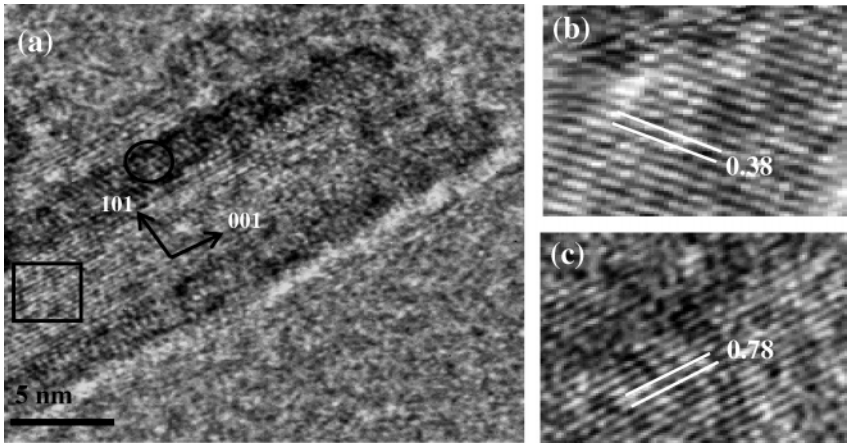

Figure 2. (a) HR-TEM image of single TiNT-H_2O_2. (b) High magnification fringe distance in the (101) direction and (c) high magnification fringe distance in the (001) direction.

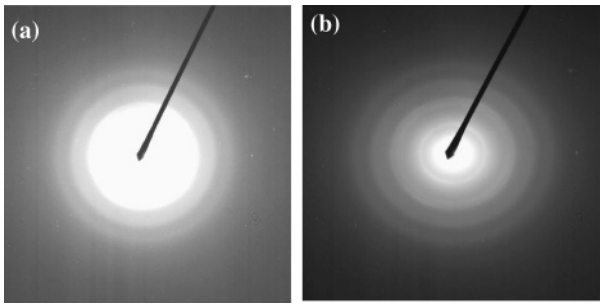

Figure 3. SAED pattern of (a) TiNT-as prepared and (b) TiNT-H_2O_2.

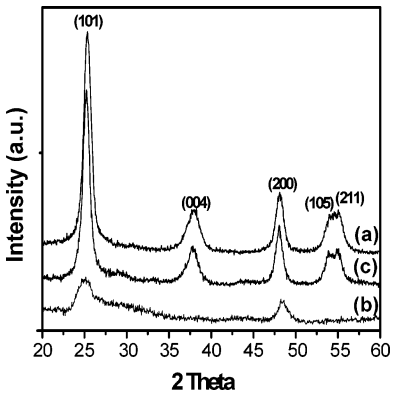

Figure 4. XRD pattern of (a) TiO_2 nanoparticles, (b) TiNT-as prepared, and (c) TiNT-H_2O_2.

TiNT-H_2O_2 exhibits clear and strong diffraction of anatase peaks at 2è 25.25, 38.5, 48.3, and 54.8/55.8°, corresponding to (101), (004), (200), and (105, 211 overlapped), respectively. The main peak was shifted slightly toward a smaller angle from 25.35° in TiNT-as prepared to 25.25° in TiNT-H_2O_2. This suggests that TiNT-H_2O_2 has smaller interchange spacing than those of TiNT-as prepared and TiO_2 nanoparticles due to the chemical environment, which results in a highly stable surface under the conditions of high oxygen chemical potentials.[23] All of the anatase characteristic peaks in TiNT-H_2O_2 are observed at levels as high as those of high crystalline titania nanoparticles. However, the anatase characteristic peaks at 38.5 and 54.8/55.8° were not observed in TiNT-as prepared due to the nature of very low crystallinity. This low crystallinity of TiNT-as prepared is consistent with a less prominent diffraction pattern of SAED (Figure 3) due to the incomplete destructive interference in scattering directions, resulting in the absence of less intense peaks at (004) and (105, 211 overlapped) in TiNT-as prepared.

TABLE 1: BET Surface Area and Chemical Composition of TiNT-as Prepared and TiNT-H_2O_2

	TiNT-as prepared	TiNT-H_2O_2
BET surface area	97.9 m^2/g	93.0 m^2/g
chemical composition[a]		
Ti K (atomic %)	35.0	33.7
O K (atomic %)	62.3	66.3
Na K (atomic %)	2.7	not detected

[a] Obtained from TEM-EDX.

This kind of ultrahigh crystalline TiNT-H_2O_2 with only the anatase phase was not prepared by any thermal treatment of TiNT-as prepared, even at high temperatures. The high temperature thermal treatment of TiNT-as prepared gave rise to a structural change to the rutile phases. The surface areas of titania nanotubes were slightly affected before and after H_2O_2 treatment, even though there was a significant change of crystallinity. It is possible to demonstrate that the peroxo species introduced in H_2O_2 treatment caused the compensation of oxygen vacancies and the activation of the lattice oxygen of TiNT-as prepared, resulting in ultrahigh crystalline TiNT-H_2O_2.

Table 1 shows the chemical composition of TiNTs obtained from the TEM-EDX spectra in Figure 5. In TiNT-as prepared, titanium (35.0%), oxygen (62.3%), and sodium (2.7%) are main elements, and trace peaks of silicon were observed as shown in Figure 5a. Silicon may have originated from TEOS as a preparation precursor. A significant amount of sodium, 2.7%, is present in TiNT-as prepared as a countercation, but no sodium is present in TiNT-H_2O_2. This result was also confirmed by XPS (Figure 6) studies where there were no Na1s peaks in TiNT-H_2O_2. The average atomic ratios of oxygen/titanium are 1.78 and 1.97 in TiNT-as prepared and TiNT-H_2O_2, respectively. This indicates a deficiency of oxygen in TiNT-as prepared, which might be due to the presence of sodium. However, these oxygen deficiencies were almost recovered to a stoichiometric ratio of titanium dioxide after hydrogen peroxide treatment. It has been conjectured that in nanotube formations, the resulting crystalline surface is corrupted, and Ti−O−Ti linkages of TiO_2 octahedra are broken in strong alkali solutions, leaving some oxygen vacancies in TiNT-as prepared. Meanwhile, these oxygen vacancies may be balanced due to the chemisorption in H_2O_2 treatment. XPS spectra (Figure 6) reveal band-bending effects, 0.79 eV shifts to higher binding energies after hydrogen peroxide treatment. This band bending effect is believed to be due to oxygen adsorption on the oxygen deficient sites in TiNT-as prepared. It was reported that the filling of an oxygen vacancy and oxygen adatom[24] caused the formation of a Ti^{4+}:O^{2-}

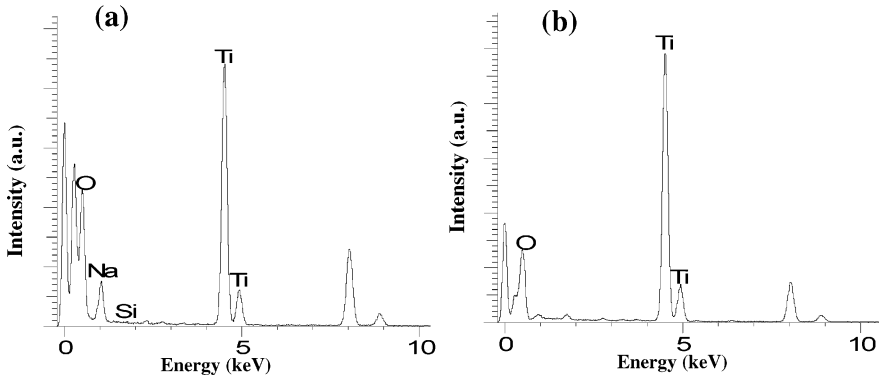

Figure 5. TEM-EDX spectra of (a) TiNT-as prepared and (b) TiNT-H_2O_2.

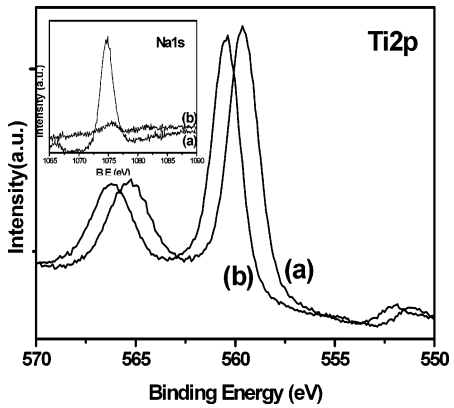

Figure 6. XPS spectra of Ti2p and Na1s (inset) of (a) TiNT-as prepared and (b) TiNT-H_2O_2.

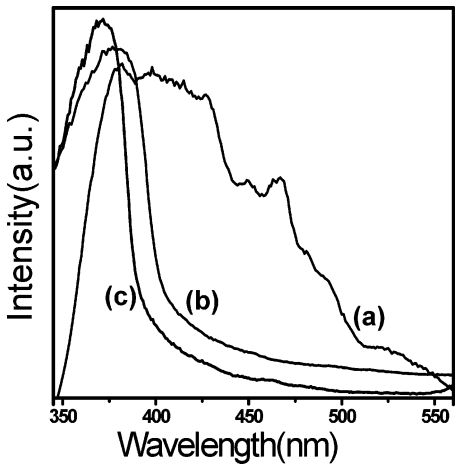

Figure 7. PL spectra of (a) TiO_2 nanoparticles, (b) TiNT-as prepared, and (c) TiNT-H_2O_2.

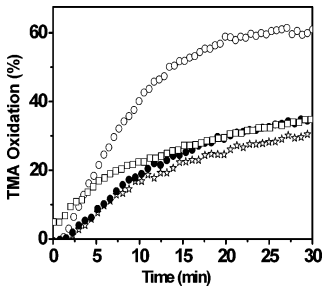

Figure 8. Photocatalytic oxidation of TMA gas over (□) TiO_2-P25 (Degussa), (☆) synthesized TiO_2 nanoparticles, (●) TiNT-as prepared, and (○) TiNT-H_2O_2.

complex[25] and resulted in a band shift to higher binding energies of the whole TiO_2 spectra.[26] There is almost no change in the shape of Ti2p in both TiNTs, indicating the same basic constitution of TiNTs. The surface defects are categorized as oxygen vacancies, impurities, and shear planes at surfaces.[27] In the case of oxygen vacancies, it is still not clear which kinds of terminations prevail. In the nanotubes, either TiNT-H_2O_2 or TiNT-as prepared, the formation of $Na_2Ti_3O_7$ can be excluded, as the interlayer spacing in $Na_2Ti_3O_7$ is ca. 84 nm, which is different from our case. Moreover, no phases of sodium titanate were observed in XRD patterns (Figure 4), and a sodium-to-titanium ratio could not be assigned to sodium titanate (Table 1).

Photoluminescence (PL) is an extremely useful tool for obtaining information about the electronic, optic, and photoelectric properties of materials. To examine the photoelectric properties of the nanomaterials, PL spectra were measured for TiO_2 nanoparticles and TiNTs excited at 310 nm at room temperature as shown in Figure 7. The PL spectrum of TiNT-H_2O_2 showed a sharp and high intense peak at 355 nm as compared to TiNT-as prepared. A broad PL spectrum of TiO_2 nanoparticles may be due to the large particle size and various kinds of prevailing defects. The main spectral bands of synthesized TiO_2 nanoparticles, TiNT-H_2O_2 and TiNT-as prepared at 355, 360, and 370 nm, are ascribed to self-trapped excitons localized on TiO_6 octahedra, respectively.[28] It is known that the red shift take places in the reduced form of titania by oxygen vacancies as observed in TiNT-as prepared.[29] Therefore, the blue shift in TiNT-H_2O_2 indicates the recovery of oxygen vacancies in TiNT-as prepared by hydrogen peroxide treatment. Also, Serpone et al.[30] reported that the PL bands of TiO_2 anatase crystals at the long wavelength range (442, 455, 465, and 502 nm) were attributed to oxygen vacancies. There are trace oxygen vacancy peaks (around 465 nm) on TiNT-H_2O_2 in contrast to TiNT-as prepared and TiO_2 nanoparticles where significant vacancies were observed. These PL results clearly indicate the recovery of oxygen vacancies of TiNT-as prepared by hydrogen peroxide treatment.

TMA as a volatile organic compound was used for the probe reactant to examine the photocatalytic oxidation activities of TiO_2-P25 (Degussa), synthesized TiO_2 nanoparticles, TiNT-as prepared, and TiNT-H_2O_2. In Figure 8, TMA oxidation efficiency of TiNT-H_2O_2 is about 2-fold higher than that of TiNT-as prepared, which is obviously consistent with the much higher crystallinity of TiNT-H_2O_2. The presence of a sodium ion and oxygen defects in TiO_6 octahedra may affect the photocatalytic properties of TiNT-as prepared. There are some arguments on the effects of the sodium ion in the photocatalytic reaction: the presence of the sodium ion on TiO_2 retards and enhances photocatalytic activity for the decomposition of malic acid[31] and

benzamide,[32] respectively. The oxygen vacancy in TiNT-as prepared can act as a recombination site of excitons,[33] resulting in the decreased photocatalytic activity. It should be considered that the substituted proton ion in TiNT-H_2O_2 may increase the photocatalytic activity owing to increased Bronsted acidity.[34] However, we believe that high crystallinity with decreased defects in TiNT-H_2O_2 is essential for its high activity in TMA degradation. The question of the peroxo group effect on the photocatalytic activity could be excluded because TiNTs were calcined at 350 °C, which is expected to be enough to remove most of the preadsorbed tracers including the peroxo group. This fact can be confirmed by visual observation of TiNT-H_2O_2, where the color vanishes identically with TiNT-as prepared after calcining over 250 °C.

Conclusion

Ultrahigh crystalline TiO_2 nanotubes (TiNT-H_2O_2) were synthesized by controlled hydrogen peroxide treatment of very low crystalline titania nanotubes (TiNT-as prepared) prepared with synthesized TiO_2 nanoparticles by hydrothermal methods in an aqueous NaOH solution. Thus, prepared ultrahigh crystalline TiNT-H_2O_2 showed comparable crystallinity with high crystalline TiO_2 nanoparticles. TiNT-H_2O_2 was ascertained with uniformly grown nanotubes with a multiwalled anatase phase only, an average outer diameter of ~8 nm, an inner diameter of ~5 nm, and a length 500−700 nm along the (001) direction. Consequently, the photocatalytic activity of TiNT-H_2O_2 was about 2-fold higher than that of TiNT-as prepared in the photocatalytic oxidation of trimethylamine gas under UV (254 nm) irradiation. These noble ultrahigh crystalline TiO_2 nanotubes can be applied as highly photoactive catalysts, supports, and advanced materials.

Acknowledgment. We gratefully acknowledge financial support from the Korea Industry Technology Foundation by the program of Human Resources Development for Regional Innovation and the Center for Ultramicro Chemical Process Systems (CUPS) sponsored by the Korea Science and Engineering Foundation (KOSEF). M.A.K. thanks KOSEF for financial support through the program of foreign scholarship.

References and Notes

(1) Fujishima, A.; Honda, K. *Nature* **1972**, *238*, 37.
(2) Gratzel, M. *Nature* **2001**, *414*, 338.
(3) Fujishima, A.; Rao, T. N.; Tryk, D. A. *J. Photochem. Photobiol., C* **2000**, *1*, 1.
(4) Gopel, W.; Reinhardt, G.; Baltes, H.; Gopel, W.; Hesse, Eds. *Sensors Update*; Wiley, New York, 1996; p 47.
(5) Skubal, L. R.; Meshkov, N. K.; Vogt, M. C. J. *Photochem. Photobiol., A* **2002**, *148*, 103.
(6) Hagfeldt, A.; Gratzel, M. *Chem. Rev.* **1995**, *95*, 49.
(7) Anpo, M.; Shima, T.; Kubokawa, Y. *Chem. Lett.* **1985**, 1799.
(8) Dresselhaus, M. S.; Dresselhauss, G.; Eklund, P. C. *Science of fullerenes and carbon nanotubes*; Academic: San Diego, 1996.
(9) Satio, R.; Dresselhaus, G.; Dreselhaus, M. S. *Physical properties of carbon nanotubes*; Imperial College Press: London, 1998.
(10) Tans, S. J. *Nature* **1998**, *393*, 49.
(11) Hoyer, P. *Langmuir* **1996**, *12*, 1411.
(12) Kasuga, T.; Hiramatsu, M.; Honson, A.; Sekino, T.; Niihara, T. *Langmuir* **1998**, *14*, 3160.
(13) Du, G. H.; Chen, Q.; Che, R. C.; Yuan, Z. Y.; Peng, L. M. *Appl. Phys. Lett.* **2001**, *79*, 3702.
(14) Davis, M. E. *Nature* **2002**, *417*, 813.
(15) Inagaki, S.; Guan, S.; Ohsuna, T.; Terasaki, O. *Nature* **2002**, *416*, 304.
(16) Hu, S.; Willey, R. J.; Notari, B. *J. Catal.* **2003**, *220*, 240.
(17) (a) Selhofer, H. *Vacuum Thin Films*; August 1999; p 15. (b) Garfunnkel, E., Gusev, E., Vul, A., Eds.; *Fundamental aspects of dielectrics on silcon based devices, NATO Science Series*; Kluwer Acaedemic Publishers: Dordrecht, The Netherlands, 1998. (c) Sambrano, J. R.; Andres, J.; Beltran, A.; Sensato, F. R.; Leite, E. R.; Stamato, L. G. F. M.; Longo, E. *Int. J. Quantum Chem.* **1997**, *65*, 625. (d) Gratzel, M. *Nature* **1992**, *353*, 737.
(18) Chemsedine, A.; Moritz, T. *Eur. J. Inorg. Chem* **1999**, *2*, 235.
(19) (19) Seifert, G.; Kohler, T.; Tenne, R. *J. Phys. Chem. B* **2002**, *106*, 2497.
(20) Henry, M.; Jolivet, J. P.; Livage, *J. Struct. Bonding* **1992**, *77*, 155.
(21) (21) Moritz, T.; Reiss, J.; Diesner, K.; Su, D.; Chemseddine, A. *J. Phys. Chem. B* **1997**, *101*, 8052.
(22) Seo, D.-S.; Lee, J.-K.; Kim, H. *J. Cryst. Growth* **2001**, *229*, 428.
(23) Wang, X.-G.; Chaka, A. M.; Scheffler, M. *Phys. Rev. Lett.* **2000**, *84*, 3659.
(24) Epling, W. S.; Peden, C. H. F.; Hendersen, M. A.; Diebold, U. *Surf. Sci.* **1998**, *412*, 333.
(25) Perkins, C. L.; Henderson, M. A. *J. Phys. Chem. B* **2001**, *105*, 3856.
(26) Diebold, U. *Surf. Sci. Rep.* **2003**, *48*, 53.
(27) (a) Yagi, E.; Hasiguti, R.; Aono, M. *Phys. Rev. B* **1996**, *54*, 7945. (b) Kofstad, P. *J. Less-Common Met.* **1967**, *13*, 635.
(28) Saraf, L. V.; Patil, S. I.; Ogale, S. B.; Sainkar, S. R.; Kshirsager, S. T. *Int. J. Mod. Phys. B* **1998**, *12*, 2635.
(29) Justicia, I.; Ordejon, P.; Canto, G.; Mozos, J. L.; Fraxedas, J.; Battiston, G. A.; Gerbasi, R.; Figueras, A. *Adv. Mater.* **2002**, *14*, 1399.
(30) Serpone, N.; Lawless, D.; Khairutdinov, R. *J. Phys. Chem.* **1995**, *99*, 16646.
(31) Fernández, A.; Lassaletta, G.; Jiménez, V. M.; Justo, A.; González-Elipe, A. R.; Herrmann, J.-M.; Tahiri, H.; Ait-Ichou, Y. *Appl. Catal., B* **1995**, *7*, 49.
(32) Bessekhouad, Y.; Robert, D.; Weber, J.-V.; Chaoui, N. *J. Photochem. Photobiol., A* **2004**, *167*, 49.
(33) Ollis, D. F.; Pelizzetti, E.; Serpone, N. *Environ. Sci. Technol.* **1991**, *25*, 1523.
(34) Ding, W.; Meitzner, G. D.; Iglesia, E. *J. Catal.* **2002**, *206*, 14.